

Charged particle densities from Au + Au collisions at $\sqrt{s_{NN}} = 130 \text{ GeV}$

BRAHMS Collaboration

I.G. Bearden^g, D. Beavis^a, C. Besliu^j, Y. Blyakhman^f, J. Brzychczyk^d, B. Budick^f, H. Bøggild^g, C. Chasman^a, C.H. Christensen^g, P. Christiansen^g, J. Cibor^c, R. Debbe^a, J.J. Gaardhøje^g, K. Grotowski^d, K. Hagel^h, O. Hansen^g, A. Holm^g, A.K. Holme^l, H. Ito^k, E. Jakobsen^g, A. Jipa^j, J.I. Jørdreⁱ, F. Jundt^b, C.E. Jørgensen^g, T. Keutgen^h, E.J. Kim^e, T. Kozik^d, T.M. Larsen^l, J.H. Lee^a, Y.K. Lee^e, G. Løvhøiden^l, Z. Majka^d, A. Makeev^h, E. McBreen^a, M. Murray^h, J. Natowitz^h, B.S. Nielsen^g, K. Olchanski^a, J. Olness^a, D. Ouerdane^g, R. Płaneta^d, F. Rami^b, D. Röhrichⁱ, B.H. Samset^l, S.J. Sanders^k, R.A. Sheetz^a, Z. Sosin^d, P. Staszek^g, T.F. Thorsteinsen^{i,l}, T.S. Tveter^l, F. Videbæk^a, R. Wada^h, A. Wieloch^d, I.S. Zgura^j,

^a Brookhaven National Laboratory, Upton, NY 11973, USA

^b Institut de Recherches Subatomiques and Université Louis Pasteur, Strasbourg, France

^c Institute of Nuclear Physics, Krakow, Poland

^d Jagiellonian University, Krakow, Poland

^e Johns Hopkins University, Baltimore, MD 21218, USA

^f New York University, New York, NY 10003, USA

^g Niels Bohr Institute, University of Copenhagen, Denmark

^h Texas A&M University, College Station, TX 77843, USA

ⁱ Department of Physics, University of Bergen, Bergen, Norway

^j University of Bucharest, Romania

^k Department of Physics and Astronomy, University of Kansas, Lawrence, KS 66045, USA

^l Department of Physics, University of Oslo, Oslo, Norway

Received 17 August 2001; received in revised form 6 November 2001; accepted 6 November 2001

Editor: P. Schiffer

Abstract

We present charged particle densities as a function of pseudorapidity and collision centrality for the $^{197}\text{Au} + ^{197}\text{Au}$ reaction at $\sqrt{s_{NN}} = 130 \text{ GeV}$. An integral charged particle multiplicity of 3860 ± 300 is found for the 5% most central events within the pseudorapidity range $-4.7 \leq \eta \leq 4.7$. At mid-rapidity an enhancement in the particle yields per participant nucleon pair is observed for central events. Near to the beam rapidity, a scaling of the particle yields consistent with the “limiting fragmentation”

E-mail address: ssanders@ku.edu (S.J. Sanders).

¹ Deceased.

picture is observed. Our results are compared to other recent experimental and theoretical discussions of charged particle densities in ultra-relativistic heavy-ion collisions. © 2001 Elsevier Science B.V. All rights reserved.

PACS: 25.75.Dw

Multiplicity distributions of emitted charged particles provide a fundamental measure of the ultra-relativistic collisions now accessible experimentally using the Relativistic Heavy-Ion Collider (RHIC). The particle densities are sensitive to the relative contribution of “soft” processes, involving the longer length scales associated with non-perturbative QCD mechanisms, and “hard”, partonic processes [1,2]. The total number of charged particles and the angular dependence of the charged particle distribution is expected to depend markedly on the amount of hadronic rescattering, the degree of chemical and thermal equilibration, and the role of subnucleonic processes.

In this Letter we present charged particle distributions in $dN_{\text{ch}}/d\eta$ with $-4.7 \leq \eta \leq 4.7$ for $^{197}\text{Au} + ^{197}\text{Au}$ collisions at $\sqrt{s_{NN}} = 130$ GeV. The pseudo-rapidity variable η can be expressed in terms of the scattering angle θ , with $\eta = -\ln[\tan(\theta/2)]$. The data were measured at the RHIC facility using complementary subsystems of the BRAHMS experiment. We have also investigated the systematics of the pseudo-rapidity distributions as a function of collision centrality. The collision centrality can be related to the number of participant nucleons in the reaction, thus allowing for comparison of different nuclear systems based on simple nucleon–nucleon superposition models [3], as has been done, for example, at lower SPS energies for the Pb + Pb system [4,5]. Our results complement those recently reported by the PHOBOS [6,7] and PHENIX [8] Collaborations by establishing global $dN_{\text{ch}}/d\eta$ systematics through a very different experimental arrangement than used in those experiments.

The BRAHMS detector system [9] consists of forward- and mid-rapidity magnetic spectrometers, which allow for the determination of charged particle properties over a wide rapidity and momentum range, and a number of global detectors employed to characterize the general features of the reaction, such as the overall charged particle multiplicity and the flux of spectator neutrons at small angles. The current analysis is based primarily on the global de-

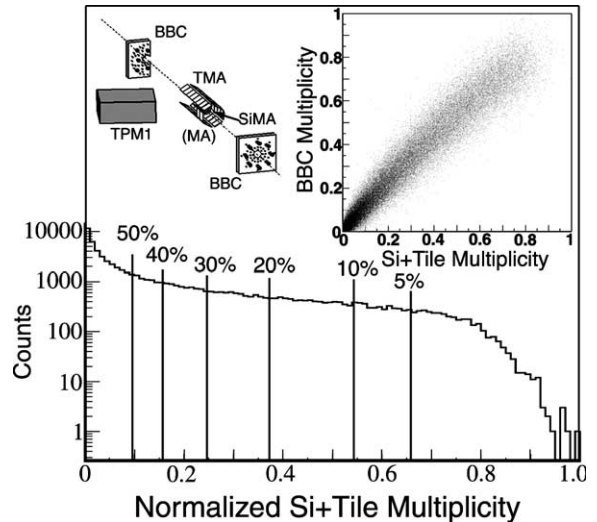


Fig. 1. Normalized MA array multiplicity distribution, as discussed in the text. The scatter plot insert shows the correlation of the normalized BBC and MA multiplicities. A schematic drawing of the global detectors used in the measurement, excluding the ZDCs, is also shown.

tectors (see Fig. 1), including the Multiplicity Array (MA), the Beam–Beam counter arrays (BBC), and the Zero-Degree Calorimeters (ZDC) [10]. Also, the front time-projection chamber (TPM1) of the mid-rapidity spectrometer arm, which is an integral part of this spectrometer, provides independent confirmation of the particle densities at selected angles.

The MA is used to determine charged particle densities in the pseudorapidity range of $-2.2 \leq \eta \leq 2.2$ for collisions at the nominal vertex. This pseudorapidity coverage is increased to $-3.0 \leq \eta \leq 3.0$ by using an extended range of vertex locations. For the present data, the collision vertex distribution was found to be roughly Gaussian in shape with $\sigma = 70$ cm. The MA consists of two layers of detectors arranged as six-sided coaxial barrels about the beam axis. The inner barrel (SiMA) is comprised of 25, 4 cm × 6 cm × 300 μm Si strip detectors located 5.3 cm from the nom-

inal beam axis, with each detector segmented into 7 strips with a 0.86 cm pitch. For the SiMA, three sides were populated with six wafers each, covering 42 segments in pseudorapidity, one side was populated with five wafers, and the last two sides were populated with one wafer, each. The outer barrel (TMA) consists of 38, 12 cm × 12 cm × 0.5 cm plastic scintillator “tile” detectors [11] located 13.9 cm from the beam axis. The scintillator tile array had four rows fully populated with 8 detectors, each, one row had 4 detectors, and the last row had 2 detectors.

The single-particle response of the SiMA and TMA elements was calibrated by selecting peripheral collision events where energy peaks corresponding to the passage of single particles, mostly pions, through the detectors could be compared to the calculated energies for these peaks based on GEANT simulations [12] and assuming nominal detector thicknesses. The uncertainty in the single-particle response is estimated as ≈5% based on the scatter of measurements for a given detector element for different vertex locations and based on the uncertainty in the GEANT simulations.

For more central collisions at RHIC, the modest segmentation of the MA results in multiple particles passing through individual detector elements. The number of particles passing through each element is determined by dividing the total energy observed in that element by the corresponding average energy loss for a single particle, primarily either a pion, kaon, or proton, as determined by GEANT simulations. Near to mid-rapidity and for central collisions an average of 10 particles pass through the Si elements and 61 particles traverse the tile elements. Two different event simulators, HIJING [13] and Fritiof [14], were used to check the sensitivity of the analysis procedure to the assumed primary particle distributions and the corresponding momentum distributions. The deduced particle multiplicities using the different codes agree to better than 3%. This uncertainty is folded into the quoted overall systematic uncertainties. The particle yields are corrected for background contributions using the GEANT simulations of the array response. These corrections are position dependent and range from 20% to 40% for the TMA and from 6% to 25% for the SiMA, increasing with increasing $|\eta|$.

The BBC Arrays consist of two sets of Cherenkov UV transmitting plastic radiators coupled to photo-

multiplier tubes. They are positioned around the beam pipe on either side of the nominal interaction point at a distance of 2.15 m. One array consists of 8 “large” detectors with 51 mm diameter phototubes and 36 “small” detectors with 19 mm diameter phototubes, arranged symmetrically around the beam pipe. The other array is asymmetric to allow the movement of the forward spectrometer to small angles and consists of 5 large detectors and 30 small detectors. The BBC elements have an intrinsic time resolution of 65 ps allowing for the determination of the position of the interaction point with a precision of ≈1.6 cm. Charged particle multiplicities in the pseudorapidity range $2.1 \leq |\eta| \leq 4.7$ are deduced from the number of particles hitting each tube, as found by dividing the measured ADC signal by that corresponding to a single particle hitting the detector. Corrections for background events were based on GEANT simulations, with the correction factors ranging from 37% to 50% of the measured yield, depending on vertex location.

The two ZDCs, positioned on either side of the nominal interaction point at a distance of 18 m, were used to establish a minimum bias trigger for the experiment. The ZDCs, which consist of alternating layers of tungsten and fiber-ribbon plastic scintillator, measure the energy deposited by spectator neutrons that are emitted at small angles with respect to the beam direction, with $|\theta| < 2$ mrad [10]. The time difference between the two ZDC signals can be used to determine the interaction vertex with a precision of ≈3.6 cm.

In addition to the global detector measurements, charged particle multiplicities were also obtained at 40°, 60°, and 90°, corresponding to $\eta = 1.1, 0.55$, and 0.0, respectively, using the TPM1 counter. This detector, which is operated in a field-free region, has an active volume of $(w, h, d) = (37.5 \text{ cm}, 21.0 \text{ cm}, 36.0 \text{ cm})$ with its volume center located 94.5 cm from the nominal vertex. For TPM1, particle multiplicities are deduced by counting reconstructed tracks arising from collision vertices within 15 cm of the nominal vertex position. The acceptance in η for this counter, accounting for both the geometric acceptance and the range of vertex locations, varies from $\Delta\eta = 0.5$ at 90° to $\Delta\eta = 0.60$ at 40°. Through the track reconstruction, the interaction vertex can be located to better than 0.5 cm. A correction for the background of secondary particles was found by projecting the vertical position

of tracks in TPM1 back to the beamline. The resulting spectrum was fitted with the sum of three Gaussian distributions; one for the peak of primary particles and summed background contributions from weak decays or secondary interactions, and delta electrons from the beampipe, respectively. The ratio of the integral of the signal peak to the two background distributions was taken as the fraction of primary particles. Typical background-to-total ratios of $\approx 5\%$ were found at all angles.

The dominant systematic uncertainties for the TPM1 measurements arise from the background subtraction and a tracking efficiency correction. The efficiency correction is obtained by inserting simulated single tracks into actual data events and analyzing the reconstruction probability using the same track reconstruction code employed for the experimental results. The tracking efficiency in the TPM1 counter ranges from almost unity for low density, peripheral scattering events, to ≈ 0.9 for central events at 90° and ≈ 0.85 for central events at 40° . In contrast, the dominant systematic uncertainty near mid-rapidity for the SiMA and TMA arrays reflect the single-particle response calibrations obtained for the constituent detectors of these arrays. At larger pseudorapidity values, the uncertainty in the background subtraction also becomes significant. In addition, the relatively thick scintillator elements of the TMA array are expected to be somewhat sensitive to beam related background that does not come from the collision vertex. These effects lead to the somewhat larger uncertainty quoted for the TMA as compared to the SiMA. The BBC systematic uncertainty is dominated by the background correction. Overall, the systematic uncertainties for the different detector systems are: SiMA, $\pm 8\%$ for $\eta < 1.5$, increasing to $\pm 10\%$ for $\eta \geq 2.5$; TMA, $\pm 12\%$ for $\eta < 1.5$ increasing to $\pm 15\%$ for $\eta \geq 2.0$; BBC, $\pm 10\%$; TPM1, $+9\%/-7\%$ for the most central events and $\pm 6\%$ for the most peripheral.

The centrality selection for the experiment was obtained by developing a minimum-biased multiplicity distribution using the MA, reflecting all events for which there is a nuclear interaction, and assuming that a cut on the total multiplicity translates to a cut on collision centrality. Fig. 1 shows the multiplicity distribution of charged particles established by the MA, normalized to the maximum observed multiplicity. The independent multiplicity measurements of the SiMA

and TMA detectors are summed for this figure, after the SiMA multiplicity was rescaled to account for the difference in the geometric coverage of the two arrays. Where possible, the location of the interaction vertex was determined using TPM1. Otherwise, the vertex determined from the BBC or ZDC data was adopted. The charged particle densities reported in this Letter are obtained almost exclusively using the TPM1 and BBC vertices and are relatively insensitive to the specific choice. The multiplicity distribution requires that a coincidence occurs between the two ZDC detectors, an interaction vertex be located within 30 cm of the array center (as obtained by one of the three possible vertex measurements), and that a TMA multiplicity of at least four be observed. The TMA multiplicity cut eliminates events corresponding to beam-gas interactions and for cases where tails of pedestals for individual detector elements add to simulate real collision events. Based on HIJING simulations, where the shape of the multiplicity distribution for events with fewer than 200 tile hits is used to estimate the missing yield for events with fewer than four tile hits, it is estimated that the TMA array observes cleanly 95% of the total nuclear cross sections. This value is used to correct for the missing cross section where the tile multiplicity is less than four when determining the final multiplicities.

Centrality selection in the BBC analysis was done using the multiplicity distribution obtained by summing the hits in the BBC arrays. This allows for the use of interaction vertices within 120 cm of the MA center, well outside the range for which the MA multiplicities could be reliably determined. The insert in Fig. 1 shows the strong correlation of the BBC and MA multiplicities, normalized to their maximum values. In the pseudorapidity range of $3.0 \leq \eta \leq 4.2$, where it was possible to analyze the BBC data using both centrality selections, the two analyses give identical results to within 1%. Still, the lower segmentation of the BBC arrays leads to a less precise multiplicity measurements as compared to the MA.

Fig. 2 presents the measured $dN_{\text{ch}}/d\eta$ distributions for a number of centrality cuts. The points associated with positive pseudorapidity values correspond to detectors located on the forward spectrometer side of the BRAHMS apparatus. Within the quoted systematic uncertainties, good agreement is found among the measurements using different detector systems. There

Table 1

Charged particle densities in $dN_{\text{ch}}/d\eta$ as a function of centrality and pseudorapidity. Total uncertainties, dominated by the systematics, are indicated. The average number of participants $\langle N_{\text{part}} \rangle$ is given for each centrality class based on HIJING model calculations. The last column gives the integral charged particle multiplicity within the pseudorapidity range $-4.7 \leq \eta \leq 4.7$

Centrality	$\langle N_{\text{part}} \rangle$	$\eta = 0$	$\eta = 1.5$	$\eta = 3.0$	$\eta = 4.5$	N_{ch}
0–5%	352	553 ± 36	554 ± 37	372 ± 37	107 ± 15	3860 ± 300
5–10%	299	447 ± 29	454 ± 31	312 ± 36	94 ± 13	3180 ± 250
10–20%	235	345 ± 23	348 ± 25	243 ± 27	79 ± 10	2470 ± 190
20–30%	165	237 ± 16	239 ± 16	172 ± 18	59 ± 8	1720 ± 130
30–40%	114	156 ± 11	159 ± 11	117 ± 13	43 ± 6	1160 ± 90
40–50%	75	98 ± 7	104 ± 7	77 ± 9	30 ± 4	750 ± 60

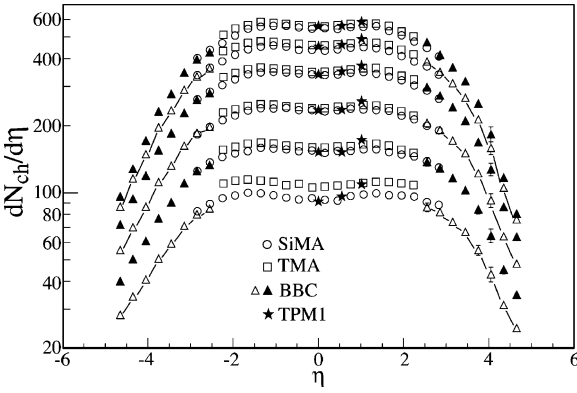


Fig. 2. Distributions of $dN_{\text{ch}}/d\eta$ for centrality ranges of, top to bottom, 0–5%, 5–10%, 10–20%, 20–30%, 30–40%, and 40–50%. Statistical uncertainties are shown where larger than the symbol size. The connecting lines and alternating open and closed symbols for the BBC data are to help distinguish points associated with different centrality ranges.

is, however, an offset observed for the TMA data which may reflect non-collision related background events. The other detectors are relatively insensitive to such a background mechanism.

Particle densities at selected pseudorapidities are tabulated in Table 1. This table also presents the integrated charge-particle multiplicities in the range $-4.7 \leq \eta \leq 4.7$. For central events at mid-rapidity, the observed particle densities are about 1.8 times greater than observed for central events in Pb + Pb scattering at $\sqrt{s_{NN}} = 17.2$ GeV [4].

The PHOBOS [6] and PHENIX [8] experiments have recently reported values for the charged particle densities at mid-rapidity corresponding to the 6%

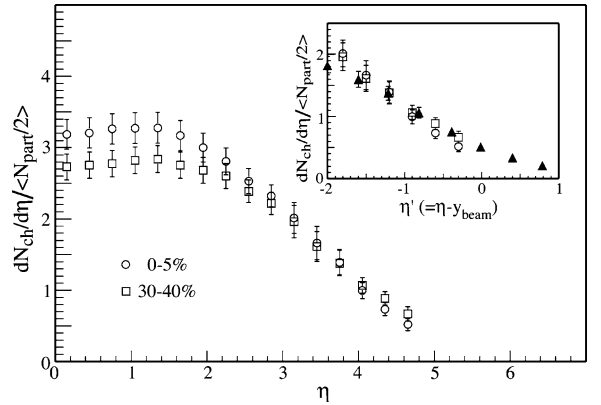


Fig. 3. Charged particle densities normalized to the number of participant pairs. Total (statistical + systematic) uncertainties are shown, not including the uncertainty in $\langle N_{\text{part}} \rangle$ (see text). The insert compares the 0–5% central (open circles) and 30–40% central (open squares) Au + Au results to the 9.4% central Pb + Pb data (closed triangles) of Ref. [4]. For this comparison of the “projectile” regions for the two reactions, the data are plotted in terms of the pseudorapidity shifted by the beam rapidity, as discussed in the text. For the insert, the particle densities are normalized to the number of projectile participants, which is equal to the number of participant pairs for a symmetric reaction.

most central events. PHOBOS obtains $dN_{\text{ch}}/d\eta|_{\eta=0} = 555 \pm 12(\text{stat}) \pm 35(\text{syst})$ while PHENIX finds $dN_{\text{ch}}/d\eta|_{\eta=0} = 609 \pm 1(\text{stat}) \pm 37(\text{syst})$. For the same centrality range, our result is $dN_{\text{ch}}/d\eta|_{\eta=0} = 549 \pm 1(\text{stat}) \pm 35(\text{syst})$. Within the systematic uncertainties the three experiments are in agreement.

Fig. 3 shows the charged-particle multiplicity distributions scaled by half of the average number of participant nucleons for the 0–5% and 30–40% central-

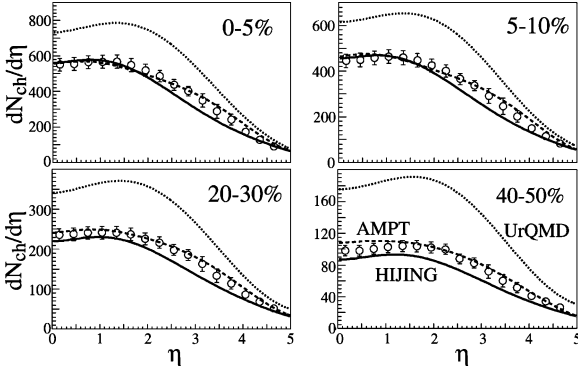


Fig. 4. Distribution of $dN_{ch}/d\eta$ for the indicated centrality ranges. Total uncertainties are indicated. HIJING, AMPT, and UrQMD model calculations are shown.

ity cuts. The average number of participants ($\langle N_{part} \rangle$) corresponding to the different centrality cuts was obtained using the HIJING code [13], where the collision geometry is based on the Glauber model [15]. The uncertainty in $\langle N_{part} \rangle$ largely reflects the uncertainty in the multiplicity measurement and is estimated as $<0.5\%$ for 5% centrality, increasing to 4% at 50% centrality. For Fig. 3 (and Fig. 4), the $dN_{ch}/d\eta$ distributions have been symmetrized and uncertainty weighted averages have been developed for the different global detector subsystems. It is found that near mid-rapidity, the charged-particle yield per participant pair is significantly greater for more central events as compared to peripheral events. However, at larger pseudorapidities, this difference disappears. The mid-rapidity behavior is consistent with that observed by the PHENIX [8] and PHOBOS [7] Collaborations and attributed [8] to an increased contribution of harder scattering processes for more central collisions.

The insert in Fig. 3 shows the Au + Au results for large pseudorapidity in terms of the pseudorapidity shifted by the beam rapidity, thus allowing for a comparison with SPS Pb + Pb data [4] within the “limiting fragmentation” picture [16]. This hypothesis states that at high energies the number of particles produced by the “wounded projectile” nucleons should be independent of the details of the “target”, the “projectile”, and the beam energy. When shifted by the beam rapidity, effectively translating to the beam’s reference frame (assuming similar values for the pseudorapidity and rapidity variables), the normalized yields near $\eta' (= \eta - y_{beam}) = 0$ should be system and en-

ergy independent. A “limiting fragmentation” behavior has been observed in pp , $p\bar{p}$, p -emulsion, and π -emulsion data (see references 34–37 of Ref. [4]). It is shown in Ref. [4] that the hypothesis also works in comparing Pb + Pb data at $\sqrt{s_{NN}} = 17.2$ GeV with 200 GeV/nucleon O + AgBr and S + AgBr results [17]. The closed triangles in the Fig. 3 insert show the Pb + Pb results. Inspection of this figure, where the current results at $\sqrt{s_{NN}} = 130$ GeV follow the same general curve as found for the lower energy data, suggests that the “limiting fragmentation” picture is successful over a very large range of energies extending from SPS to RHIC ($\sqrt{s_{NN}} = 17.2$ GeV to 130 GeV). The absence of a centrality dependence for the scaled yields near beam rapidity, as seen in Fig. 3, is also consistent with such a picture.

In Fig. 4 we compare HIJING [13], UrQMD [18], and AMPT model [19–21] calculations to the data for different centrality ranges. HIJING is a model that places special emphasis on perturbative QCD processes leading to multiple minijet production from parton scatterings. The model, which does not include final state rescattering except for schematic jet quenching, is found to do a good job in describing the data at mid-rapidity, but underestimates the widths of the multiplicity distributions at all centralities. The AMPT model uses HIJING to generate the initial phase space of partons, but then extends the calculations to model the parton–parton collisions and the final hadronic interactions. By including these final state interactions, the widths of the multiplicity distributions are found to agree well with experiment, suggesting the importance of these final state interactions. It is also interesting to note that the LUCIFER code [22] gives similar results to AMPT but within a purely hadronic formulation. The UrQMD transport model accounts for hadronic interactions at low and intermediate energies in terms of interactions between known hadrons and their resonances and at higher energies in terms of excitations of color strings and their subsequent fragmentation. For the present RHIC data, the shape of the pseudorapidity distributions are well reproduced, however with the particle production being way too large. The current results appear to rule out the UrQMD model as a description of the RHIC data.

The BRAHMS experiment has measured pseudorapidity densities of charged particles from Au + Au collisions at $\sqrt{s_{NN}} = 130$ GeV over a large range of

pseudorapidity as a function of collision centrality using several independent detector systems and methods. We observe an enhancement of particle production for central collisions at mid-rapidity, suggesting a breakdown in the simple scaling by the number of participant nucleons seen at larger pseudorapidities. Comparisons of the Au + Au fragmentation region data with SPS energy Pb + Pb results suggest that a “limiting fragmentation” behavior is seen for nucleus–nucleus collisions and is, in fact, already reached at the lower energy. With the inclusion of final hadronic interactions, parton scattering models are found to give a good description of the observed behaviors.

Acknowledgements

The BRAHMS Collaboration wishes to thank the RHIC team for their efforts leading to the successful startup of the collider and for the support they have given to the experiment. This work was supported by the Division of Nuclear Physics of the Office of Science of the US Department of Energy under contracts DE-AC02-98-CH10886, DE-FG03-93-ER40773, DE-FG03-96-ER40981, and DE-FG02-99-ER41121, the Danish Natural Science Research Council, the Research Council of Norway, the Jagiellonian University Grants, the Korea Research Foundation Grant, and the Romanian Ministry of Education and Research (5003/1999, 6077/2000).

References

- [1] X.-N. Wang, M. Gyulassy, Phys. Rev. Lett. 86 (2001) 3496.
- [2] K.J. Eskola, K. Kajantie, K. Tuominen, Phys. Lett. B 497 (2001) 39, hep-ph/0009246.
- [3] A. Bialas, M. Bleszyński, W. Czyż, Nucl. Phys. B 111 (1976) 461.
- [4] P. Deines-Jones et al., Phys. Rev. C 62 (2000) 014903, hep-ex/9912008.
- [5] M.M. Aggarwal et al., Eur. Phys. J. C 18 (2001) 651, nucl-ex/0008004.
- [6] B.B. Back et al., Phys. Rev. Lett. 85 (2000) 3100, hep-ex/0007036.
- [7] B.B. Back et al., nucl-ex/0105011;
B.B. Back et al., nucl-ex/0106006.
- [8] K. Adcox et al., Phys. Rev. Lett. 86 (2001) 3500.
- [9] D. Beavis et al., Conceptual Design Report for BRAHMS, BNL-62018;
I.G. Bearden et al., in preparation.
- [10] C. Adler, A. Denisov, E. Garcia, M. Murray, H. Strobele, S. White, Nucl. Instrum. Methods Phys. Res. A 461 (2001) 337, nucl-ex/0008005.
- [11] S. Aota et al., Nucl. Instrum. Methods Phys. Res. A 352 (1995) 557.
- [12] GEANT 3.2.1, CERN program library.
- [13] X. Wang, M. Gyulassy, Phys. Rev. D 44 (1991) 3501, code HIJING 1.36.
- [14] H. Pi, Comput. Phys. Commun. 71 (1992) 173.
- [15] R.J. Glauber, G. Matthiae, Nucl. Phys. B 21 (1970) 135.
- [16] J. Benecke, T.T. Chou, C.N. Yang, E. Yen, Phys. Rev. 188 (1969) 2159.
- [17] A. Dabrowska et al., Phys. Rev. D 47 (1993) 1751.
- [18] S.A. Bass et al., Prog. Part. Nucl. Phys. 41 (1998) 255, nucl-th/9803035.
- [19] B. Zhang, C.M. Ko, B.-A. Li, Z. Lin, Phys. Rev. C 61 (2001) 067901.
- [20] Z.-W. Lin, S. Pal, C.M. Ko, B.-A. Li, B. Zhang, Phys. Rev. C 64 (2001) 011902(R).
- [21] Z.-W. Lin, S. Pal, C.M. Ko, B.-A. Li, B. Zhang, nucl-th/0105044;
Z.-W. Lin, private communication.
- [22] D.E. Kahana, S.H. Kahana, Phys. Rev. C 63 (2001) 031901(R).